Reflective ghost imaging with classical Gaussian-state light

Deyang Duan (段德洋) and Yunjie Xia (夏云杰)*

Shandong Provincial Key Laboratory of Laser Polarization and Information Technology, Research Institute of Laser, Qufu Normal University, Qufu 273165, China

**Corresponding author: yjxia@mail.qfnu.edu.cn*

Received July 25, 2011; accepted September 27, 2011; posted online November 18, 2011

In this letter, we use quantum description and the Gaussian state to study reflective ghost imaging with two classical sources, and to provide their expressions. We find that the reflective ghost imaging of a rough-surfaced object, using Gaussian-state phase-insensitive or classically correlated phase-sensitive light, can be expressed in terms of the phase-insensitive or phase-sensitive cross-correlations between the two detected fields, including a background term. Moreover, reflective ghost imaging with two classical Gaussian-state lights is shown to have similar features as spatial resolution and field of view.

OCIS codes: 110.0110, 270.0270, 030.0030.
doi: 10.3788/COL201203.031102.

Ghost imaging is a procedure to indirectly form the image of an object by photocurrent correlation. This procedure is called ghost imaging because the photons that provide the spatial information of the object does not interact directly with the object to be imaged. Transmission ghost imaging utilizes three sources: maximally entangled phase-sensitive light (e.g., the output of ideal spontaneous parametric down-conversion)[1−3], classically correlated phase-sensitive light (e.g., two laser with phase-conjugate modulations imposed on them)[4], and phase-insensitive light (e.g., pseudothermal or true thermal state light)[5−7].

Considering the reflective ghost imaging configuration, an optical source generates a signal beam and a reference beam by a beam splitter. The signal beam does not interact with the object of interest. After free-space propagation, its transverse power distribution is measured using a high-spatial-resolution detector. The reference beam interacts with the object after the free-propagation and is measured by a bucket detector. Cross-correlating the photocurrents from the two detectors yields the ghost image, the physical origin of which lies in a perfect correlation between the spatial fluctuations imposed by the source plane on the signal and the reference beams.

Most ghost imaging experiments have been performed in transmission[1,6−8], and nearly all ghost imaging theories have addressed the transmission case. However, reflective ghost imaging is more valuable in application, such as in the remote sensing technology. Preliminary tabletop experiments have demonstrated the feasibility of reflective ghost imaging[9,10]. Several works in reflective ghost imaging have been achieved using Gaussian-state pseudothermal and quantum light[11]. However, little exploration has been conducted on reflective ghost imaging with two classical sources by quantum description, including a comparison of their features. The Gaussian-states offer both a practically relevant and a theoretical convenient framework for studying ghost imaging[11−13]; thus, we utilize the Gaussian state in this letter.

The configuration considered for reflective ghost imaging is shown in Fig. 1. An optical source generates two scalar, quasi-monochromatic, paraxial, positive-frequency optical fields: a signal field $\widehat{E}_{\rm S}(x,t)\mathrm{e}^{-\mathrm{i}\omega_0 t}$ and a reference field $\widehat{E}_{\rm R}(x,t)\mathrm{e}^{-\mathrm{i}\omega_0 t}$, with $\sqrt{\text{photons}/\text{m}^2 s}$ units and a common center frequency ω_0. Here, x is the transverse coordinate. The commutation relations within this paraxial approximation for the base-band field operators are[14]

$$\left[\widehat{E}_m(x_1,t_1),\widehat{E}_{\rm l}(x_2,t_2)\right]=0, \tag{1}$$

$$\left[\widehat{E}_m(x_1,t_1),\widehat{E}^{\dagger}_{\rm l}(x_2,t_2)\right]=\delta_{ml}\delta(x_1-x_2)\delta(t_1-t_2), \tag{2}$$

where m, l = S, R; δ_{ml} is the Kronecker delta function; $\delta(\cdots)$ is the unit impulse.

The reference beam illuminates a rough-surfaced planar object $L-$ meters away from the beam splitter. The light reflected from the object is then collected by a bucket detector after the $L-$ meters' free-space propagation. The signal light illuminates the high-spatial-resolution detector (CCD array) after the $L-$ meters' free-space propagation, from which a 1 : 1 ghost image is formed.

The photocurrents from the bucket detector and each pixel on the CCD array are sent to a correlator with coincidence measurement, of which the output for the CCD pixel located at transverse coordinate x_1 is given by

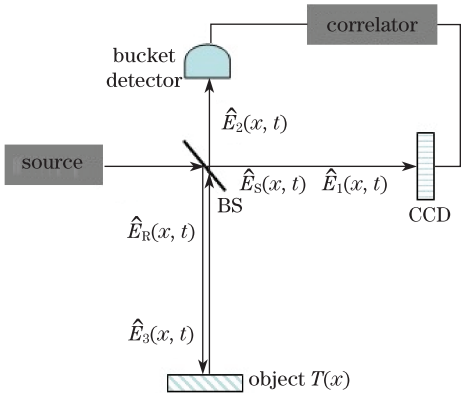

Fig. 1. Setup for reflective ghost imaging.

$$\widehat{C}(x_1) = \frac{1}{T_1}\int_{-\frac{T_1}{2}}^{\frac{T_1}{2}} \widehat{I}_1(t)\widehat{I}_2(t)\mathrm{d}t, \tag{3}$$

where T_1 is the averaging time. We suppress a L/c time delay in $\widehat{I}_1(t)$ needed to account for the delay incurred by the reflective light from the object.

Considering two ideal photodetectors assumed to have identical subunity quantum efficiencies and finite electrical bandwidths, no dark current or thermal noise contributes to the output current. The classical output currents from the two detectors corresponding to the following quantum measurements are given by[15,16]

$$\widehat{I}_m(t) = q\int \mathrm{d}u \int_{A_m} \mathrm{d}x \widehat{E}^{\dagger}_{\eta,m}(x,u)\widehat{E}_{\eta,m}(x,u)h_{\mathrm{B}}(t-u), \tag{4}$$

where $m = 1, 2$, A_1, and A_2 denote the area of one pixel in the signal arm and the photosensitive surface of the bucket detector; q is the electron charge; $h_{\mathrm{B}}(t)$ is a real impulse response to model the real detector's finite electrical bandwidth.

$$\widehat{E}_{\eta,m}(x,t) = \sqrt{\eta}\widehat{E}_m(x,t) + \sqrt{1-\eta}\widehat{E}_{\mathrm{vac},m}(x,t), \tag{5}$$

where $m = 1, 2$ and $\sqrt{\eta}$ are the detector's quantum efficiencies; $\widehat{E}_{\mathrm{vac},\,m}$ is a vacuum-state field operator.

$$\widehat{E}_1(x,t) = \int \mathrm{d}x' \widehat{E}_{\mathrm{S}}(x',t)h_{\mathrm{l}}(x-x'), \tag{6}$$

$$\widehat{E}_2(x,t) = \int \mathrm{d}x' \widehat{E}_3(x',t)h_{\mathrm{l}}(x-x')T(x'), \tag{7}$$

$$\widehat{E}_3(x,t) = \int \mathrm{d}x' \widehat{E}_{\mathrm{R}}(x',t)h_{\mathrm{l}}(x-x'). \tag{8}$$

Here, $h_{\mathrm{l}}(x)$ is the Huygens–Fresnel–Green's function:

$$h_{\mathrm{l}}(x) \equiv \frac{k_{0\mathrm{e}}^{\mathrm{i}k_0(L+|x|^2/2L)}}{2\mathrm{i}\pi L}, \tag{9}$$

where $k_0 = \omega_0/c$ is the wave number associated with the center frequency and $T(x')$ is the object's field-reflection coefficient. We have neglected the time delays.

The objects of interest for reflective ghost imaging will have microscopic surface variations (i.e., from a nominal, smooth surface profile) whose standard deviations can greatly exceed the illumination wavelength and whose transverse correlation scale can be of subwave length. When such a surface is illuminated by laser light, a laser speckle arises in the object return. Here, we use a statistical model for $T(x)$[17]:

$$\langle T^*(x_1)T(x_2)\rangle = \lambda_0^2 T(x_1)\delta(x_1-x_2), \tag{10}$$

where λ_0 is the center wavelength of the illumination field; $T(x_1)$ is physically the mean square speckle reflection coefficient at location x_1, which is the object information sought.

The $\widehat{C}(x_1)$ measurement yields an unbiased estimate of the ensemble-average equal-time photocurrent cross-correlation function:

$$\begin{aligned}\left\langle \widehat{C}(x_1)\right\rangle &= \left\langle \widehat{I}_1(t)\widehat{I}_2(t)\right\rangle \\ &= A_1\lambda_0^2 q^2\eta^2 \int \mathrm{d}u_1 \int \mathrm{d}u_2 \int_{A_2} \mathrm{d}x' \int \mathrm{d}x_2 \\ &\quad\times \left\langle \widehat{E}_1^{\dagger}(x_1,u_1)\widehat{E}_1(x_1,u_1)E_2^{\dagger}(x_2,u_2)\widehat{E}_2(x_2,u_2)\right\rangle \\ &\quad\times \mathrm{T}(x_2)h_{\mathrm{l}}^*(x'-x_2)h_{\mathrm{l}}(x'-x_2) \\ &\quad\times h_{\mathrm{B}}(t-u_1)h_{\mathrm{B}}(t-u_2).\end{aligned} \tag{11}$$

We use the commutation relations (1) and (2) to put the integrand into normal order. Subsequently, the Gaussian-state moment-factoring theorem is utilized to the fourth-order moment[12,18], replacing the fourth-order moment with expressions that depend only on the second-order moments of the fields.

$$\begin{aligned}\left\langle \widehat{C}(x_1)\right\rangle &= \frac{A_1A_2\lambda_0^2q^2\eta^2}{L^2}\int \mathrm{d}u_1 \int \mathrm{d}u_2 \int \mathrm{d}x_2 \\ &\quad\times \Big(\left\langle \widehat{E}_1^{\dagger}(x_1,u_1)\widehat{E}_1(x_1,u_1)\right\rangle \\ &\quad\times \left\langle \widehat{E}_2^{\dagger}(x_2,u_2)\widehat{E}_2(x_2,u_2)\right\rangle \\ &\quad+ \left|\left\langle \widehat{E}_1^{\dagger}(x_1,u_1)\widehat{E}_2(x_2,u_2)\right\rangle\right|^2 \\ &\quad+ \left|\left\langle \widehat{E}_1(x_1,u_1)\widehat{E}_2(x_2,u_2)\right\rangle\right|^2 \Big) \\ &\quad\times \mathrm{T}(x_2)h_{\mathrm{B}}(t-u_1)h_{\mathrm{B}}(t-u_2).\end{aligned} \tag{12}$$

Thus far, we have opted for the quantum description of reflective ghost imaging configuration. We now proceed with the details for each of the two sources.

We calculate the lensless reflective ghost imaging with phase-insensitive light. We consider the phase-insensitive correlation propagation in two limiting regimes: the near field, which corresponds to the region in which diffraction effects are negligible, and the far field, in which diffraction spread is dominant. For phase-insensitive coherence propagation, a single Fresnel number $D_0 = k_0x_0a_0/2L$ distinguishes these regimes; $D_0 >> 1$ corresponds to the near field and $D_0 << 1$ corresponds to the far field[19]. Here, when a_0 is the beam radius, x_0 is the coherence radius.

With phase-insensitive light, the signal and reference fields have the maximum phase-insensitive cross-correlations, but no phase-sensitive cross-correlation[13].

$$\left\langle \widehat{E}_m^{\dagger}(x_1,t_1)\widehat{E}_l(x_2,t_2)\right\rangle = K_{m,l}^{(n)}(x_1,x_2)R_{m,l}^{(n)}(t_2-t_1), \tag{13}$$

$$\left\langle \widehat{E}_m(x_1,t_1)\widehat{E}_l(x_2,t_2)\right\rangle = 0, \tag{14}$$

where m, $l = 1$, 2 and the superscripts (n) labeled normally are the ordered phase-insensitive terms. Substituting Eqs. (13) and (14) into Eq. (12), we obtain

$$\left\langle \widehat{C}(x_1)\right\rangle = C_0(x_1) + C_n\int \mathrm{d}x_2 |K_{1,2}^{\prime(n)}(x_1,x_2)|^2\, T(x_2), \tag{15}$$

where

$$C_0(x_1) = \frac{A_1 A_2 \lambda_0^2 q^2 \eta^2}{L^2} \cdot R_{1,1}^{(n)}(0) R_{2,2}^{(n)}(0) \Big[\int h_B(t) \mathrm{d}t \Big]^2 K_{1,1}^{\prime(n)}(x_1, x_2) \cdot \int K_{2,2}^{\prime(n)}(x_2, x_2) T(x_2) \mathrm{d}x_2. \quad (16)$$

This is a featureless background term of reflective ghost imaging.

$$C_n = \frac{A_1 A_2 \lambda_0^2 q^2 \eta^2}{L^2} \left[\left| R_{1,\,2}^{(n)}(t) \right|^2 * h_{\mathrm{B}}(t) * h_{\mathrm{B}}(-t) \right]_{t=0.} \quad (17)$$

The second part on the right in Eq. (15) is the reflective ghost image term. Here, "$*$" denotes convolution. The signal and reference fields are taken for the Gaussian-Schell model[20]. In the near field, we obtain the maximum phase-insensitive cross-correlation as given by

$$K_{m,l}^{(n)}(x_1,\, x_2) R_{m,l}^{(n)}(t_2 - t_1) = \frac{2P}{\pi a_0^2} \cdot \mathrm{e}^{\mathrm{i}k_0(|x_2|^2 - |x_1|^2)/2L} \mathrm{e}^{-(|x_1|^2 + |x_2|^2)/a_0^2 - |x_2 - x_1|^2/2x_0^2} \cdot \mathrm{e}^{-(t_2 - t_1)^2/2T_0^2}, \quad (18)$$

where T_0 is the coherence time.

Substituting Eq. (18) into Eq. (15), we obtain the following phase-insensitive reflective ghost imaging expression:

$$\left\langle \widehat{C}(x_1) \right\rangle = C_0(x_1) + C_n \Big(\frac{2P}{\pi a_0^2} \Big)^2 \cdot \int \mathrm{e}^{-2(|x_1|^2 + |x_2|^2)/a_0^2 - |x_1 - x_2|^2/x_0^2} T(x_2)\, \mathrm{d}x_2. \quad (19)$$

Here, the phase term is removed in the integrand.

With the Gaussian-Schell model source, Eq. (19) shows that the reflective ghost image in near field has the field of view a_0. The finite cross-correlation coherence length x_0 limits the spatial resolution of the image.

The reflective ghost imaging with the phase-insensitive light is in the far-field regime, in which $D_0 << 1$. Due to the diffraction effect, the second-order correlation functions must be propagated from the source plane to the detection planes. Fortunately, for Gaussian-Schell model correlation functions, this transformation is a simple replacement of a_0 by $a_L = 2L/k_0 x_0$ and x_0 by $x_L = 2L/k_0 a_0$. Hence, the far-field ghost imaging of the phase-insensitive result is given by

$$\left\langle \widehat{C}(x_1) \right\rangle = C_0(x_1) + C_n \Big(\frac{2P}{\pi a_L^2} \Big)^2 \cdot \int \mathrm{e}^{-2(|x_1|^2 + |x_2|^2)/a_L^2 - |x_1 - x_2|^2/x_L^2} T(x_2)\, \mathrm{d}x_2. \quad (20)$$

As shown, the field of view increases to a_L, whereas the image spatial resolution degrades to $\sqrt{2} x_L$ in the far field of the reflective ghost imaging.

Moreover, similar fields of view and spatial resolutions were found from the previous Gaussian-state analysis for the near- and far-field transmission of the ghost imaging with a phase-insensitive source[12]. Indeed, the only difference between Eqs. (19) and (20) and the corresponding result for the transmission case is the factor $A_2 \lambda_0^2 / L^2$, which appears in the former.

We have now completed the reflective ghost imaging in the near and far fields with phase-insensitive light. We then calculate the reflective ghost imaging with classically correlated phase-sensitive light.

In the current section, we calculate the expressions of lensless reflective ghost imaging with classically correlated phase-sensitive light in the near and far fields.

The phase-sensitive correlation function propagates in a different manner from its phase-insensitive counterpart. We find that the coherence radius diffraction and intensity radius diffraction are decoupled in this case[21]. Two Fresnel numbers are required to distinguish the near field from the far field: the Fresnel number for the diffraction of the coherence radius, $D_{\mathrm{N}} = k_0 x_0^2 / 2L$, and the Fresnel number for diffraction of the intensity radius, $D_{\mathrm{F}} = k_0 a_0^2 / 2L$. The near-field regime for the phase-sensitive correlation propagation occurs when both Fresnel numbers are far greater than one, and the far-field regime is when both Fresnel numbers are much less than one[12]. Both conditions are more stringent than the corresponding one for the phase-insensitive light.

Unlike in the phase-insensitive case, the signal and reference field have phase-sensitive cross-correlations, but no phase-insensitive cross-correlation. With Gaussian-Schell model and the near field, the phase-sensitive cross-correlation is given by[20]

$$\left\langle \widehat{E}_1(x_1,\, t_1) \widehat{E}_2(x_2,\, t_2) \right\rangle = K_{1,2}^{(p)}(x_1,\, x_2) R_{1,\,2}^{(p)}(t_2 - t_1) = \frac{2P}{\pi a_0^2} \mathrm{e}^{\mathrm{i}k_0(|x_2|^2 + |x_1|^2)/2L} \cdot \mathrm{e}^{-(|x_1|^2 + |x_2|^2)/a_0^2 - |x_2 - x_1|^2/2x_0^2} \cdot \mathrm{e}^{-(t_2 - t_1)^2/2T_0^2}, \quad (21)$$

where the superscripts (p) labeled normally represent the ordered phase-sensitive term.

Substituting Eq. (21) into Eq. (15), we obtain the phase-sensitive reflective ghost imaging expression in the near field:

$$\left\langle \widehat{C}(x_1) \right\rangle = C_0(x_1) + C_p \Big(\frac{2P}{\pi a_0^2} \Big)^2 \cdot \int \mathrm{e}^{-2(|x_1|^2 + |x_2|^2)/a_0^2 - |x_2 - x_1|^2/x_0^2} T(x_2)\, \mathrm{d}x_2, \quad (22)$$

where

$$C_p = \frac{A_1 A_2 \lambda_0^2 q^2 \eta^2}{L^2} \left[\left| R_{1,\,2}^{(p)}(t) \right|^2 * h_{\mathrm{B}}(t) * h_{\mathrm{B}}(-t) \right]_{t=0}. \quad (23)$$

For the Gaussian-Schell model source, forming the near-field reflective ghost image with the classically correlated phase-sensitive light identical with the near-field reflective ghost image formed with the phase-insensitive light, with the exception of the near field condition for

phase-sensitive coherence propagation, is far more stringent than that for its phase-insensitive counterpart.

When the source-to-object separation is the far-field regime for phase-sensitive coherence propagation, the source-plane phase-sensitive cross-correlation that resulted in the preceding near-field ghost image gives rise to the following detection-plane phase-sensitive cross-correlation[21]

$$K_{1,2}^{(p)}(x_1, x_2)R_{1,2}^{(p)}(t_2 - t_1) = \frac{2P}{\pi a_L^2} \cdot \mathrm{e}^{\mathrm{i}k_0(|x_2|^2+|x_1|^2)/2L}\mathrm{e}^{-(|x_1|^2+|x_2|^2)/a_L^2-|x_2+x_1|^2/2x_L^2} \cdot \mathrm{e}^{-(t_2-t_1)^2/2T_0^2}. \quad (24)$$

Substituting Eq. (24) into Eq. (15), we obtain the expression of reflective ghost imaging with classically correlated phase-sensitive light in far field.

$$\left\langle \widehat{C}(x_1) \right\rangle = C_0(x_1) + C_p\Big(\frac{2P}{\pi a_L^2}\Big)^2 \cdot \int \mathrm{e}^{-2(|x_1|^2+|x_2|^2)/a_L^2-|x_2+x_1|^2/x_L^2} T\,(x_2)\,\mathrm{d}x_2. \quad (25)$$

The reflective ghost image with classically correlated phase-sensitive light in the far field is an inverted version of the corresponding reflective ghost image with phase-insensitive light in the far field. They have identical fields of view and spatial resolution.

Identical fields of view and spatial resolution are evident between the reflective ghost imaging and the transmission ghost imaging with phase-sensitive light in near and far field.

In conclusion, we use quantum description and Gaussian-state to explore the reflective ghost image in near and far field with phase-insensitive light and classically correlated phase-sensitive light. We find the reflective ghost image formation to be due to phase-insensitive or phase-sensitive cross-correlations between the signal and reference fields. Similar features of the reflective ghost image with phase-insensitive light and classically correlated phase-sensitive light include the fields of view and spatial resolution. However, the phase-sensitive coherence propagation is much more stringent than the phase-insensitive case. Thus, the reflective ghost imaging with phase-insensitive light performs better than the classically correlated phase-sensitive light in the experiment.

This work was supported by the National Natural Science Foundation of China (No. 61178012) and the Specialized Research Fund for the Doctoral Program of Higher Education (No. 20093705110001).

References

1. T. B. Pittman, Y. H. Shih, D. V. Strekalov, and A. V. Sergienko, Phys. Rev. A **52,** 3429 (1995).
2. B. I. Erkmen and J. H. Shapiro, Phys. Rev. A **78,** 023835 (2008).
3. S.-H. Tan, B. I. Erkmen, V. Giovannetti, S. Guha, S. Lloyd, L. Maccone, S. Pirandola, and J. H. Shapiro, Phys. Rev. Lett. **101,** 253601 (2008).
4. J. H. Shapiro and B. I. Erkmen, Opt. Soc. Am. ICQI, IthD1 (2007).
5. A. Gatti, E. Brambilla, M. Bache, and L. A. Lugiato, Phys. Rev. Lett. **93,** 093602 (2004).
6. F. Ferri, D. Magatti, A. Gatti, M. Bache, E. Brambilla, and L. A. Lugiato, Phys. Rev. Lett. **94,** 183602 (2005).
7. P. Zhang, W. Gong, X. Shen, S. Han, and R. Shu, Phys. Rev. A **80,** 033827 (2009).
8. L. Gao, S. Zhang, J. Xiong, S. Gan, L. J. Feng, D. Z. Cao, and K. Wang, Phys. Rev. A **80,** 021806 (2009).
9. R. Meyers, K. S. Deacon, and Y. Shih, Phys. Rev. A **77**, 041801(R) (2008).
10. C. Wang, D. Zhang, Y. Bai, and B. Chen, Phys. Rev. A **82,** 063814 (2010).
11. N. D. Hardy, "Analyzing and Improving Image Quality in Reflective Ghost Imaging" ADA545213 (2011).
12. B. I. Erkmen and J. H. Shapiro, Phys. Rev. A **77,** 043809 (2008).
13. B. I. Erkmen and J. H. Shapiro, Phys. Rev. A **79,** 023833 (2009).
14. H. P. Yuen and J. H. Shapiro, IEEE Trans. Inf. Theory **IT-24,** 657 (1978).
15. H. P. Yuen and J. H. Shapiro, IEEE Trans. Inf. Theory **IT-26,** 78 (1980).
16. J. H. Shapiro, Proc. SPIE **5111,** 382 (2003).
17. J. H. Shapiro, B. A. Capron, and R. C. Harney, Appl. Opt. **20,** 3292 (1981).
18. L. Mandel and E. Wolf, *Optical Coherence and Quantum Optics* (Cambridge University Press, Cambridge, 1995).
19. J. W. Goodman, *Statistical Optics* (Wiley, New York, 2000).
20. B. I. Erkmen and J. H. Shapiro, Adv. Opt. Photon. **2,** 405 (2010).
21. B. I. Erkmen and J. H. Shapiro, Proc. SPIE **6305,** 63050G (2006).